The Autism Risk Factor CHD8 Is a Chromatin Activator in Human Neurons and Functionally Dependent on the ERK-MAPK Pathway Effector ELK1

Bahareh Haddad Derafshi
Institute for Stem Cell Biology and Regenerative Medicine
Tamas Danko
Institute for Stem Cell Biology and Regenerative Medicine
Soham Chanda
Institute for Stem Cell Biology and Regenerative Medicine
Pedro Batista
Center for Personal Dynamic Regulomes
Ulrike Litzenburger
Center for Personal Dynamic Regulomes
Qian Yi Lee
Institute for Stem Cell Biology and Regenerative Medicine
Yi Han Ng
Department of Molecular and Cellular Physiology
Anu Sebin
Institute for Stem Cell Biology and Regenerative Medicine
Howard Y. Chang
Center for Personal Dynamic Regulomes
Thomas C. Südhof
Department of Molecular and Cellular Physiology
Marius Wernig (wernig@stanford.edu)
Institute for Stem Cell Biology and Regenerative Medicine

Research Article

Keywords: Autism Risk Factor, CHD8, Chromatin Activator, Human Neurons, ERK-MAPK Pathway, ELK1, autism spectrum disorder (ASD)

Posted Date: August 18th, 2021

DOI: https://doi.org/10.21203/rs.3.rs-799225/v1

The Autism Risk Factor CHD8 Is a Chromatin Activator in Human Neurons and Functionally Dependent on the ERK-MAPK Pathway Effector ELK1

Bahareh Haddad Derafshi[1,3], Tamas Danko[1,3], Soham Chanda [1,2], Pedro Batista[5,8] , Ulrike Litzenburger[5,9], Qian Yi Lee[1,3], Yi Han Ng[1,2] , Anu Sebin[1,3], Howard Y. Chang [4,5,6,7], Thomas C. Südhof [2,4], Marius Wernig* [1,3]

[1]Institute for Stem Cell Biology and Regenerative Medicine, [2]Department of Molecular and Cellular Physiology, [3]Department of Pathology, [4]Howard Hughes Medical Institute, [5] Center for Personal Dynamic Regulomes, [6]Program in Epithelial Biology[7,] Department of Genetics, 265 Campus Drive, Stanford, CA, 94305, USA

[8]Current address: Laboratory of Cell Biology, Center for Cancer Research, National Cancer Institute, National Institutes of Health, Bethesda, MD 20892, USA

[9]Current address: Celgene, San Francisco, CA, 94158, USA.

* Correspondence: wernig@stanford.edu

Abstract

The chromodomain helicase DNA-binding protein CHD8 is among the most frequently found de-novo mutations in autism spectrum disorder (ASD)[1-4]. Despite its prominent disease involvement, little is known about its molecular function in the human brain. CHD8 is believed to be a chromatin regulator, but mechanisms for its genomic targeting is also unclear. To elucidate the role of CHD8 in human neurons, we generated conditional loss-of-function alleles in pluripotent stem cells. Chromatin accessibility and transcriptional profiling showed that *CHD8* is a potent chromatin opener and transcriptional activator of its direct neuronal targets, including a distinct group of ASD genes. We found the chromatin targeting of CHD8 to be highly context dependent. In human neurons, CHD8 was preferentially bound at promoter sequences

which were significantly enriched in ETS motifs. Indeed, the chromatin state of ETS motif-containing promoters was preferentially affected upon loss of CHD8. Among the many ETS transcription factors, we found ELK1 to be the best correlated with CHD8 expression in primary human fetal and adult cortical neurons and most highly expressed in our ES cell-derived neurons. Remarkably, ELK1 was necessary to recruit CHD8 specifically to ETS motif-containing sites. These findings imply the functional cooperativity between ELK1, a key downstream factor of the MAPK/ERK pathway, and CHD8 on chromatin involvement in human neurons. THEREFORE, the MAPK/ERK/ELK1 axis may also play a role in the pathogenesis caused by *CHD8* mutations [5].

Main

To study the role of CHD8 in human neurons, we engineered the *CHD8* locus in pluripotent stem cells to produce heterozygous and homozygous conditional knockout (cKO) cells. The heterozygous cKO allele was constructed by surrounding exon 4 with two loxP sites (Fig. 1a, Extended Data Fig. 1a). Deletion of exon four is predicted to produce a frameshift and early termination mutation. We identified two correctly targeted embryonic stem (ES) and one correctly targeted induced pluripotent (iPS) cell line (Extended Data Fig. 1b-c). To generate a homozygous cKO of *CHD8*, we used CRISPR/Cas9 to introduce an indel mutation in the non-targeted wild-type allele of heterozygous cKO cells (Fig. 1b, Extended Data Fig. 1h, i). This effort resulted in two homozygous cKO ES and one iPS cell line (Extended Data Fig. 1j).

The single-cell RNA sequencing data from the middle temporal gyrus of human cortex [6] revealed *CHD8* is predominantly expressed in excitatory neurons; therefore, we decided to conditionally deplete CHD8 protein in human neurons using our previously published Ngn2 differentiation method (Fig. 1c) [7]. We infected engineered neurons with lentiviral vectors encoding Cre recombinase or ΔCre- an inactive recombinase, and we confirmed successful protein depletion by Western blotting and immunofluorescence (Fig. 1d, Extended Data Fig. 1g,k). Importantly, depletion of CHD8 in

differentiated neurons did not affect overall cell viability (Extended Data Fig. 1k). Therefore, we could conduct an in-depth characterization of the cell biological consequences of loss of CHD8 in human neurons.

Electrophysiological assays revealed the basic non-synaptic properties of CHD8-mutant neurons were not obviously altered. Intrinsic membrane properties of neurons were unchanged in both heterozygous and homozygous *CHD8*-mutant cells (Extended Data Fig. 1l, p). Active membrane properties induced by stepwise current injection were similar between the heterozygous and homozygous mutants and the respective control cells (Extended Data Fig. 1m, q). Additionally, the frequency and amplitude of spontaneous miniature EPSCs in CHD8 heterozygous cKO cells were not statistically different from WT neurons (Extended Data Fig. 1o). Similarly, we found that evoked excitatory postsynaptic currents (EPSCs) were unchanged in heterozygous and homozygous mutant cells compared to respective control cells (Extended Data Fig. 1n, r). Thus, loss of *CHD8* did not grossly affect the intrinsic physiological and basic functional synaptic properties of human neurons using standard electrophysiology.

Given CHD8's proposed role as chromatin regulator, we evaluated the transcriptional effects following CHD8 depletion [8]. Quantification of gene expression by RNA-sequencing showed that heterozygous *CHD8* mutant cells exhibited only subtle changes than WT cells, as described before (Fig. 1e) [9,10]. Gene expression changes were much more pronounced in homozygous *CHD8*-mutant neurons (Fig. 1f). Overall, downregulation of genes was more pronounced than upregulation in the homozygous KO cells, and more DEGs (differentially expressed genes) were downregulated than upregulated (Fig. 1f). The overlap between heterozygous and homozygous KO cells was also higher among the downregulated genes, suggesting CHD8 predominantly is an activator of gene expression in neurons (Fig. 1g). The enrichment analysis for molecular, cellular, biological, and disease pathways showed a significant overrepresentation of pathways involved in molecular regulations of chromatin, transcription, and pathways related to ERK/MAPK signaling and cell adhesion molecules (Extended Data Fig. 1s).

Accordingly, disease pathway enrichment and disease-associated Gene Set Enrichment Analysis (GSEA) analysis showed an enrichment of gene signature for neurodevelopmental diseases and ASD (Fig. 1h, Extended Data Fig. 1t,u)[11].

To map the chromatin targeting of CHD8 in human neurons, we generated a human embryonic stem (ES) cell line in which we tagged the endogenous CHD8 gene with a C-terminal FLAG-HA-tag (Fig. 2a, Extended Data Fig. 2a-d). Western blotting showed that the tagged protein had the expected size of CHD8 (Fig. 2b). We performed chromatin immunoprecipitation followed by sequencing (ChIP-seq) upon differentiation of ES cells into neurons using antibodies for both HA and the N-terminus of the CHD8 protein. There was a good correlation between the ChIP-seq with the two antibodies (Pearson r^2 =0.80, Extended Data Fig. 2e,f). Conversely, the correlation of CHD8 binding with a published ChIP-seq dataset from neural progenitor cells was low [10] (Pearson r^2 =0.25) (Extended Data Fig. 1f). These observations suggest genomic binding of CHD8 is strongly context-dependent.

Classification of CHD8 binding revealed a distinct enrichment around the proximal promoters and little binding at distal regulatory sites (Fig. 2d, Extended Data Fig. 2g)[12]. Further characterization employing ENCODE repository of histone ChIP-seq data from H9-derived and human primary neurons revealed that the sites of CHD8 binding promoters (n=3,600) overlap with active histone marks (Fig. 2e, Extended Data Fig. 2i,j). The ontology of the associated genes with those promoters is related to regulating chromatin, transcription, and translation (Extended Data Fig. 2h) [13].

Motif enrichment analysis showed that CHD8 binding sequences in human neurons are enriched for the ETS and YY1 motifs, and the odds ratio of the enrichment of ETS motifs was significantly higher in the strong binding sites of CHD8 compared to weaker binding sites (Fig. 2f, Extended Data Fig. 2k)[14]. Non-CHD8 occupied promoters lacked such enrichment (Extended Data Fig. 2l, m).

We then investigated the functional consequences on the local chromatin at CHD8 target sites in response to CHD8 depletion. Changes activating or repressive binding of CHD8 by analyzing transcriptional changes of associated genes with CHD8-bound promoters in response to CHD8 depletion. RNA-sequencing between control and CHD8 KO cells in the cumulative distribution of CHD8-bound and unbound genes showed that loss of CHD8 leads to downregulation of its target genes, suggesting CHD8 primarily acts as a transcriptional activator of its direct target genes (Fig. 2g). Indeed, a comparison of odds ratios for CHD8 binding at promoters of up-regulated and down-regulated genes in heterozygous and homozygous mutant cells using RNA-seq validated the finding. Conversely, we also found that CHD8 binding is stronger at promoters of down-regulated genes than of up-regulated genes in both conditions (Extended Data Fig. 2n).

Among the CHD8 target genes that were predominantly downregulated were many Autism risk genes defined by the Simons Foundation Autism Research Initiative (Fig. 2h, i, Extended Data Fig. 2o). Co-expression analysis of this set of genes in single-cell RNA-seq data of the human fetal brain revealed a striking separation of the genes up-and down-regulated following CHD8 depletion suggesting a functional relationship within these two groups of genes (Fig. 2j)[6].

To characterize the presumed function of CHD8 as a chromatin remodeler in human neurons, we then performed Assay of Transposase Accessible Chromatin (ATAC)-seq to assess high-resolution chromatin accessibility of chromatin [15,16]. Differential accessibility analysis revealed the vast majority represent a loss of accessibility in CHD8-mutant cells: 1481 peaks lost accessibility, but only 106 peaks gained accessibility in KO neurons (Fig. 3a, b, see also the PCA analysis in Extended Data Fig. 3a). The ontology enrichment analysis for genes with a significantly changed ATAC-peak signal at their promoter vicinity (+/- 5 Kb) produced terms about regulation of transcription and RNA binding pathways (Fig. 3c). Motif enrichment showed there is an enrichment of CAAT (an RNA polymerase II binding sequence) and the GGAA (the ETS factor motif) at sites that lost accessibility in CHD8 knockout neurons (Fig. 3d). The CAAT-box enrichment is commonly found at core promoters [17]. However, the

enrichment of an ETS motif was intriguing since we had already found it to be enriched at CHD8 targets. We, therefore, next interrogated CHD8 binding at the dynamically regulated ATAC-seq sites. We found that CHD8 binding strongly enriched at differentially accessible promoters in particular promoters closing without CHD8 (Fig. 3e, f, Extended Data Fig. 3b). Overall, across the genome, CHD8 binding was enriched at all sites that showed differential chromatin accessibility in KO cells, compared to unchanged ATAC-seq sites (Fig. 3g). These results suggest that CHD8 regulates its chromatin targets through direct genomic interaction.

Next, we were investigating the relationship between CHD8-dependent chromatin accessibility, differential gene expression, and CHD8 chromatin binding. Averaging fold changes of all genes proximal to opening and closing ATAC-seq peak showed changes in ATAC-seq signal in KO is at the same direction as the changes of the RNA expression at the corresponding gene (Extended Data Fig. 3c). This observation was also accurate for high-confidence autism genes as defined by SFARI (Extended Data Fig. 3d). These data indicated that chromatin changes in CHD8 KO cells are, in fact, relevant and affect gene expression in neurons. We then applied a multivariate hidden Markov model (HMM) to annotate the genome-wide chromatin state of CHD8 targets using publicly available datasets for chromatin modifications of human H9-derived neurons [18,19]. First, we validated that our model accurately described the expected chromatin state at a group of well-annotated promoters (n=500) (Extended Data Fig. 3e). Next, we analyzed the enrichment of CHD8 targets, including the sites of CHD8 binding and the ATAC-seq peaks at annotated genome. Enrichment analysis revealed CHD8 regulates chromatin accessibility at regions of the genome with active chromatin state with no preference to a distinct classification or mapping to a particular genomic annotation (e.g., promoters or enhancer). In contrast, CHD8 binding displayed a strong preference for proximal promoters (Fig. 3h). To validate our annotation analysis, we analyzed CHD8 binding at the promoters of a distinct group of 136 differentially expressed genes that also in ATAC-seq KO their promoter accessibility changed. We observed CHD8 binding strongly enriched at closing promoters in downregulating genes (Fig. 3i). These results reveal CHD8 directly activates chromatin and RNA expression at its overlapping targets.

To further explore the possible role of ETS motifs guiding specificity of CHD8 interaction and effects on chromatin accessibility, we analyzed regulatory DNA sequence and motif elements in ATAC-seq target regions with or without ETS motifs. We interrogated the chromatin dynamics at the selected sites and observed a much more pronounced loss of ATAC-seq signal at the ETS motif containing sites compared to ETS motif-free regions (Fig. 4a). In combination with ETS motif enrichments in CHD8 binding sites and CHD8-dependent ATAC-Seq sites, these results suggested the possibility of a functional interaction of an ETS factor and CHD8. To further characterize ETS motif-dependent CHD8 activity, we implemented cross-correlation analysis of the ATAC-seq signal to infer nucleosome density at transcriptional start sites (TSS) with ETS motifs but not at TSS lacking ETS motifs (Fig. 4b, c)[16]. We found the altered density of the +1-nucleosome intriguing, prompting us to investigate the symmetry of CHD8 binding at promoters with and without ETS motifs. Indeed, the average CHD8 ChIP-seq signal (100 bp binned) upstream of promoters of actively transcribed genes in neurons was stronger than downstream of promoters, again specifically at ETS motif-containing sites but not others (Fig. 4d).

Which ETS factor may functionally interact with CHD8 in human neurons? First, we turned to our gene expression data from wild-type neurons. We found that among all *ETS* factors *ELK1* is most highly expressed in human neurons (Fig. 4e) [6,20]. Next, we analyzed the expression of *ETS* factors in human prefrontal cortex. Clustering analysis of single cell RNA-seq data from the human prefrontal cortex revealed a correlative gene expression pattern between *ELK1* and *CHD8* but no other *ETS* factors (Fig. 4f). These results point to the ELK1 transcription factor as potential functional partner of CHD8 and ELK1.

To examine the functional cooperativity between ELK1 and CHD8 in targeting chromatin, we constructed lentiviral vectors with short hairpin RNA (shRNA) targeting *ELK1* and *ELF4* as control. We measured the binding of CHD8 at a series of CHD8 binding, ETS motif-enriched peak regions (see the experimental diagram at the Extended Data Fig. 4a). Quantitative qPCR and western blotting confirmed

a robust decrease in mRNA and the protein after infecting the neurons with two hairpins against *ELK1* and one hairpin against *ELF4* (Extended Data Fig. 4b). We also validated the specificity of our selected ChIP-seq peaks for CHD8 binding in three independent pull-down experiments, which showed a complete absence of CHD8 binding in KO neurons (Extended Data Fig.4c, d). After these validation experiments, we then asked whether ELK1 would be required for proper CHD8 targeting and chromatin binding. To that end, we performed ChIP on selected sites based on the strength of CHD8 binding and the number of ETS motifs. The results were striking: Among all strong CHD8 binding sites interrogated that also contained ETS motifs, ELK1 knockdown reduced CHD8 binding (Fig. 4g). In contrast, CHD8 peaks that did not contain ETS motifs were unaffected. The knockdown of the other ETS factor ELF4 did not change CHD8 binding at the same peak sites (Fig. 4h). Thus, ELK1 is the critical ETS factor necessary for the proper chromatin targeting of CHD8.

Discussion

In summary, these results establish that CHD8 is responsible for maintaining an open chromatin configuration and overall transcriptional activation in human neurons. Our data also reveals functional cooperativity of *CHD8* and *ELK1* (the effector of MAPK/ERK) in chromatin regulation through a distinct model of directional activity oriented around the ELK1 motif. Additionally, we revealed CHD8 regulates a distinct group of autism genes positively correlated in expression patterns in the developing human cortex, suggesting a conserved and developmentally regulated transcriptional connectivity between CHD8 and its targets. In light of these data, it is intriguing to speculate that MAPK/ERK/ELK1 may play a functional role in developing neuropsychiatric alterations caused by *CHD8* mutations. Modulation of specific aspects of this pathway, which is known to regulate activity-dependent gene expression and synaptic plasticity, may represent a foundation to explore a therapeutic opportunity for functional interference with pathology induced by *CHD8* mutations [21,22].

Acknowledgments

We would like to thank Dr. Joanna Wysocka , Dr. Tomasz Swigut , and Dr. Daniel Jarosz for support and thoughtful discussions. This project was supported by an Howard Hughes Medical Institute Faculty Scholar Award and a New York Stem Cell Foundation Investigator Award (M.W.). T.C.S. and H.Y.C. are Investigators of the Howard Hughes Medical Institute.

Main Figure Legends

Fig. 1: Widespread transcriptional changes upon loss of CHD8 in neurons.

a, Strategy to generate a heterozygous conditional knockout (cKO) allele of *CHD8* in pluripotent stem cells. The endogenous Exon 4 was flanked with LoxP sites by AAV-mediated homologous recombination. Following correct targeting, the selection cassette was removed by transient transfection with FlpE recombinase to generate the final conditional allele. Infection with Cre recombinase leads to deletion of the floxed allele and generates CHD8 KO cells. Infection with ΔCre (an inactive form of Cre) is used throughout the study for the control condition. **b,** Generation of homozygous *CHD8* cKO cells by introducing a CRISPR transfection-mediated indel mutation into the non-conditional *CHD8* allele, which led to a frameshift mutation. Infection of a correctly targeted line with Cre recombinase generates homozygous CHD8 null cells, whereas control infection with ΔCre leaves the engineered mutations unchanged. **c,** Single-cell RNA sequencing data showing expression of CHD8 and cell-type-specific marker genes (CPM+1) in human cortical neurons (image credit: Allen Institute)[6]. **d,** Western blot from conditional heterozygous and homozygous KO neurons show a decrease and a near-complete depletion of the protein in each system. **e,** Volcano plot for RNA-seq fold change in heterozygous CHD8 KO vs. control neurons. **f**, Volcano plot for RNA-seq fold change in homozygous CHD8 KO vs. control neurons. **g,** Analysis for overlapping DEGs between the heterozygous and homozygous knockout RNA-seq experiment shows that the odds ratio of downregulated genes is significantly higher compared to overlapping upregulated genes. **h,** Disease

Ontology (DO) and enrichment analysis for DEGs from homozygous RNA-seq experiment show enrichment of genes for human diseases (left). Additionally, it shows the association of molecular and biological ontology within the group of genes involved in the pathology of intellectual disability (right)[23].

Fig. 2: CHD8 localizes to promoters enriched with ELK1 motifs.

a, Targeting strategy to insert a C-terminal FLAG-HA tag at the endogenous *CHD8* locus (see Extended Data Fig. 2a-d). **b,** Western blot analysis of tagged and non-tagged (control) ES cells using an anti-HA antibody. **c**, An example of a CHD8 peak at the promoter of the *KMT5B* locus. **d,** Pie chart shows the distribution of CHD8 ChIP-seq peaks across the genomic regions in ES cell-derived neurons. **e**, In neurons CHD8 binding sites enriched with active histone modifications (analysis of ENCODE data for H9 cell-derived neurons) [13]. **f**, Top heatmaps are CHD8 binding at overlapping peaks between two separate pull-downs of HA and CHD8 antibodies (n=3696 overlapping peaks). Using HOMER and MEME, we found ETS and YY1 motifs enriched at CHD8-bound sites. The bottom panels' heatmaps are signals from the same samples that stratified on CHD8-unbound promoters (n=4000). The greyscale shows normalized coverage for all groups [24,25]. **g**, Expression of genes with CHD8 peak at the +/- 5Kb of the promoters showed a marked decrease compared to control. **h**, Overlapping of ASD genes from SFARI-2020 list and genes with CHD8 binding at promoters[11,26]. Significance of the overlapping calculated with the hypergeometric test. **i,** Gene expression of CHD8-bound ASD genes with significant expression change in RNA-seq experiment.
j, correlation analysis of CHD8-target ASD genes (same gene set we discovered in “i”) within the human fetal cortex (12-37 CPW) is plotted. The clusters of similarly expressed genes led to the separation of the same gene modules shown in “i”. A separate module of non-CHD8 target autism gene was randomly selected for correlation analysis of the control group.

Fig. 3: CHD8 activates chromatin at its targets in neurons.

a, Heatmaps of normalized ATAC-seq signal in cKO homozygous and control neurons from a targeted ES cell line (CR1) and a targeted iPS cell line (CR3) and two technical replicates within each line. Cluster1 and Cluster 2 are separated based on unsupervised clustering analysis, which shows sites that gain or lost accessibility regions in KO and plotted the corresponding genomic annotation at each cluster. **b**, Normalized ATAC-seq signal from aggregates of Cluster1 and Cluster2 shows KO chromatin predominantly lost accessibility. **c**, Ontology analysis of the genes with differentially regulated ATAC-seq peaks in KO at the promoters' vicinity (+/- 5Kb TSS in Cluster1 +Cluster2).
d, Motif enrichment analysis in Cluster 2. **e**, Volcano plot depicting each ATAC-seq peak as one dot. The color indicates the distance of the ATAC-seq peak summit from the CHD8 peak summit at the immediate vicinity, and the size reflects the CHD8 ChIP-seq peak score. **f**, Linear regression of DE-seq2 normalized CHD8 binding signal and DE-seq2 normalized ATAC-seq signal at the promoters of genes with change accessibility, and example ASD genes are labeled. The color indicates log2 change of the accessibility in CHD8 KO. **g**, Analysis of CHD8 binding and ATAC-seq signal on sites with differential accessibility in *CHD8* KO neurons and sites with no change. The average ATAC-seq signal is calculated from control samples. **h,** Analysis of chromatin modification enrichment with ChromHMM and the annotation of the genomic feature with transition probability for 15 state model uncovers the distribution and the relative enrichment of CHD8 binding and the ATAC-seq sites across all chromatin states in neurons. **i,** RNA-seq and ATAC-seq signal for **136** genes with a significant change in gene expression and ATAC-seq signal in KO. CHD8 binding signal sorted with the same order of the sites of the promoters at the respective heatmap.

Fig. 4: Demonstration of functional cooperativity between CHD8 and ELK1 in targeting and regulating chromatin.

294 **a**, Normalized CHD8 signal and ATAC-seq signal in *CHD8*-KO and the control samples plotted, and
295 ELK1 motif density plotted as a green enrichment plot. Genome-wide ChIP-seq and ATAC-seq signal
296 divided into three groups: sites with exclusive enrichment for ELK1 motif, sites without ELK1 motif, and
297 the control sites, which are the randomly shuffled peak sets from control samples. For each group, we
298 compared the ATAC signal from KO to the control sample. **b,** Shows cross-correlation of ATAC-seq
299 signal with NucleoATAC to measure nucleosome density. The enrichment plot is a subset of calculated
300 nucleosome density signal taken from TSS with +/- ELK1 (ETS) motif (motif occurrence >1).**c**, Violin
301 plots compare normalized and averaged nucleosome density signal at 100bp region around the
302 position +1 of TSS with the presence or absence of ELK1 motif. Statistical analysis of distribution
303 comparison is calculated with the Kolmogorov Smirnov test. **d**, CHD8 binding signal taken from 100 bp
304 upstream and downstream of transcription start sites (TSS), with the presence or absence of ELK1
305 motif. **e,** Average expression of ETS factors shows ELK1 is the only highly expressed ETS gene in
306 differentiated human neurons (average FPKM values taken from wild type neurons). **f**, Gene
307 expression of *CHD8* and ETS factor analysis in human developing human cortex and unsupervised
308 clustering of expression levels (Alan brain data)[6]. **g**, ChIP-qPCR analysis for CHD8 binding after ELK1
309 is KD with two different hairpin RNAs (shRNAs). The control condition is the empty vector. The number
310 of ETS motif at each peak site indicated beneath each peak. There was no change in CHD8 binding at
311 sites without the ETS motif. See also Extended Data Fig. 4d for validation of CHD8 binding on the
312 peaks in CHD8-KO neurons. **h**, Knockdown of ELF4 does not affect CHD8 binding on either of ETS or
313 YY1 motif sites, suggesting ELF4 does not influence chromatin binding of CHD8.
314
315

316 # Methods

317 **Cell culture**

318 *CHD8*-KO human ES cells were generated from the human embryonic stem cell (ESC) line H9
319 (passage 50, WA09 WiCell Research Institute, Inc.) and an iPSC line from a male individual. Only cells

with normal karyotype were used to generate conditional knockout cells and downstream analysis. Pluripotent stem cells were maintained in mTeSR1 (STEMCELL Technologies), and small-molecule Thiazovivin (5μM) (STEMCELL Technologies) applied to the medium before single-cell passaging. The conversion of PSC to induced neurons is described below according to our previously published protocol [7].

Lentivirus generation

Production of lentivirus was according to the previously described method [27].

Production of Adeno-Associated Virus (AAV)

Recombinant adeno-associated virus (rAAV-DJ) was used to deliver the targeting vector to pluripotent stem cells. To produce rAAV we co-transfected three plasmids: 25 μg of pAAV [28], 25 μg of helper plasmid (pAd5) and 20 μg of capsid (AAV-DJ), into one T75 flask with 80% confluent HEK293T cells (ATCC) by calcium phosphate transfection method [28,29]. Two days after transfection, cells were harvested by trypsin for 10 minutes and lysed by three rounds of freeze and thawing in dry ice and water bath (37□C). The rAAV virus was collected from the supernatant by spinning the whole lysate and removal of the pellet. The virus was aliquoted in small volumes to freeze in -80ºC. Before usage for every 100 μl of supernatant, ten units of Benzonase endonuclease (EMD Chemical Inc, Merck 1.01695.002) added at (37ºC) for 5 minutes to digest DNA from HEK cells; the capsid protects AAV DNA from digestion.

Generation of human induced excitatory neurons (iN)

Human excitatory neurons differentiated from pluripotent stem cells by over-expression of lineage-specific transcription factor-Neurogenin 2 (Ngn2) as described before[7]. In summary, one day prior to conversion, we dissociated stem cells into single cells with Accutase (Innovative Cell Technologies) and seeded at ~ 40K cells into one 24 well plate pre-coated with Matrigel (BD Biosciences) in medium supplemented with Thiazovivin (5μM) (STEMCELL Technologies) and doxycycline (2 mg/ml, Clontech).

After 6 hours, we infected the cells with lentivirus containing Ngn2, RTTA, and Cre recombinase or ΔCre (truncated form of Cre which is not functional and it is used as control). The next day we replaced the medium with neuronal medium N2/DMEM/F12/NEAA (Invitrogen) containing doxycycline (2 mg/ml, Clontech). We kept the cells in this medium for 5 days, and on day 6 we added ~ 10K mouse glia cells into each 24 well and replaced the culture medium with a serum-containing medium. We analyzed the cultures approximately 3-5 weeks after induction. To generate homozygous knockout neurons, we infected the neurons with LV- Cre or ΔCre one day after induction of the Ngn2 transcription factor.

Immunofluorescence (IF)

For immunofluorescence (IF) staining of cells (embryonic stem cells and iN cells) we fixed the cells using 4% paraformaldehyde (PFA) for 15 minutes at room temperature and permeabilized the cell membrane using 5% Triton for 1 hour and then blocked the cells in a solution containing 1% BSA, 5% FBS and 1%Triton. The primary antibody was added to the same blocking buffer according to these dilutions: CHD8 antibody (Rabbit-Behtyl lab-A301-224A) used as 1:3,000, Synapsin1 antibody (Rabbit-Synaptic Systems-106002) used as 1:500, Homer1 (Rabbit-Synaptic Systems-160003) used as 1:500, HA (Rabbit-Sigma-H6908) used as 1:500, Map2 (Mouse-Sigma-M9942) used as 1:500,Tuj1 (Rabbit-Biolegened-802001) used as 1:500, ELK1 (Rabbit, Bethyl lab-A303-529A) used as 1:400 and incubated for O/N at 4ºC. DAPI added as 100 nM solution for 1 minute. The secondary antibodies were made as 1:1,000 solutions and incubated for 1hr at room temperature.

Western blotting

Human stem cells and neurons lysed with RIPA lysis buffer supplemented with 5mM EDTA and protease inhibitor (Roche), for 5 minutes at room temperature and 10 minutes on ice. After the lysis, sample buffer (4x Laemmli buffer containing 4% SDS, 10% 2-mecaptaneol, 20% glycerol, 0.004% 4-Bromophenol blue, 0.125 M Tris HCl, pH 6.8) added, and the samples either directly loaded on 4-12% SDS-PAGE gel, or froze in -80 for further analysis. For all of the immunoblots, approximately 20 to 30 µg protein was separated on an SDS-PAGE gel. Antibodies used in this manuscript used with this

dilutions: CHD8 antibody (Rabbit-Behtyl lab-A301-224A) used as 1:4,000, ELK1 (Rabbit, Bethyl lab-A303-529A) used as 1:1,000, HA (Rabbit-Sigma-H6908) used as 1:1,000, β-actin antibody (Rabbit,Abcam-ab8227) used as 1:20,000. All blots were visualized by fluorescently labeled secondary antibodies on Odyssey CLx Infrared Imager with Odyssey software (LI-COR Biosciences).

RNA-sequencing

RNA was obtained from 3 weeks-old cultures of iN cells by adding Trizol LS (Thermo Fisher Scientific) directly into cell culture well. Total 500 ng RNA processed for library preparation using "TruSeq" RNA sample preparation-V2 kit and "Ribo-Zero" rRNA removal kit (Illumina) according to manufacturer's instruction. The sequencing ran on Illumina`s NextSeq 550 system with 1x 75-bp cycle run.

RNA-seq data analysis

FastQ files were run on FastQC to obtain high quality (trimmed and cleaned) reads. The reads were aligned to human reference genome sequence (hg19) and assembled with TopHat/Bowtie (version 2.1.1)[30] for transcriptome analysis. Since we generated the library from a mix of mouse and human RNA, the resulting reads were also from a mixture of both species. We therefore aligned our reads to the human genome with stringent criteria (zero mismatches allowed). The aligned sequences were randomly sampled and re-aligned to the other species' genome (the mouse, mm9 genome) to ensure that cross-species DNA alignment is not happening. Note that ~ 1% of the reads aligned to both human and mouse genome were discarded from SAM file with SAMtools [31]. The Refseq hg19 GTF file of transcriptome annotation was downloaded from Ensembl (https://uswest.ensembl.org/index.html) and used as a reference annotation file in TopHat alignment run command to increase the speed and the sensitivity of alignments to splice junctions. Duplicate reads (which arise from PCR step during library preparation) were removed with SAMtools. Pre-built indexes of bowtie were downloaded from the "Bowtie" webpage (http://bowtie-bio.sourceforge.net/tutorial.shtml). All SAMtools subcommands were used to convert SAM files to BAM files (Bindery Alignment Map). Additionally, SAMtools were used for indexing (to view the signal on genome browser) and for sorting (necessary for downstream

analysis). Cufflinks was used for transcript assembly and to estimate the abundance (FPKM) of coding genes. To quantify transcripts across all the samples and obtain estimated counts for downstream analysis, we used HTSeq (htseq-count option) [32]. These raw counts were used as input for DESeq2 to perform differential expression analysis [33] and to generate summarizing plots.

The single cell RNA data of human brain and the bulk RNA-seq of the developing human cortex obtained from Allen Human Brain Atlas and the Image credit in figure 1 (with some modification) is the Allen Institute [6].

ChIP-seq and data analysis

ChIP-seq was performed with modifications from a published protocol [34]. In summary, ten confluent 10cm plates of iN cells (approximately $10x10^6$ neurons in total) 10 days after differentiation was used for chromatin extraction. Cultures were crosslinked with 1% Formaldehyde (Sigma) for 10 min at RT. Glycine (125mM) was added to quench and terminate the cross-linking reaction and after washing with PBS cells were scraped off the dishes and collected into a 50 mL tube. DNA samples were subjected to sonication to obtain an average fragment size of 200 to 600 bp, using Covaris (S220-Focused Ultrasonicator). After sonication, the pellets were cleared from debris by centrifugation in 4°C and the supernatant was collected for further analysis of DNA fragment size (column-purified DNA ran in 2% agarose gel to determine the size) and for DNA/protein concentration analysis. For input calculation approximately 0.5% of cross-linked chromatin separated and saved before the addition of IP antibody. For immunoprecipitation (IP) 1.5 µg anti-CHD8 or anti-HA antibody added into ChIP buffer (RIPA buffer supplemented with protease inhibitors, PMSF and 5mM EDTA) and left to rotate O/N in 4°C. At the same time protein G agarose beads (Active Motif) were washed and blocked with 5% BSA in ChIP buffer and left to rotate O/N in 4°C. The next day, the antibody bound chromatin was added to protein G and rotated 5hr in 4°C. The immunoprecipitated material was washed, and the IP material was eluted from beads with elution buffer (50 mM NaCl, Tris-HCl; pH 7.5) by vortexing at 37 °C for 30min. The eluted DNA was separated from beads with spinning. For reverse cross-linking, the IP and input

material was incubated in 65 °C/shaking along with RNaseA (10 ug/ul) and 5M NaCl plus proteinase K (20 ug/ul). DNA was purified on a column (Zymo Research) and processed for library preparation. NEBNext ChIP-seq library prep kit was used for library preparation. Sequencing was performed on Illumina`s NextSeq 550 system with 1x 75-bp cycle run. We obtained 18 to 20 million total reads per sample in one sequencing run.

ATAC-seq experiment

We followed the Pi-ATAC-seq protocol for the transposition of homozygous knockout and control neurons [35]. In summary, the cells were fixed in culture for 5 minutes, with 1% PFA and detached from the plate with EDTA and stained for GFP, which allowed us to sort the Cre-GFP positive cells. After that, the transposition proceeded as standard ATAC-seq protocol with slight modification (extra step of reverse cross-linking performed overnight in 65C°). Note that for heterozygous knockout and wild type transposition, we followed the original ATAC-seq protocol in which un-fixed nuclei is permeabilized and subjected to transposition [36].

ATAC-seq, ChIP-seq data analysis

For ChIP-seq and ATAC-seq ENCODE ChIP-seq pipline2 was used to obtain significant peaks[13,18]. For motif discovery, we used HOMER (v4.10) (http://homer.ucsd.edu/homer/). For clustering analysis, we used Cluster 3.0 [37]. Heatmaps were generated using java program-Treeview [38]. For ontology analysis, we used DAVID analytical tool [39]. To obtain estimated counts within the region of interest in ATAC-seq experiment we used FeatureCounts- a general-purpose read count tool from Rsubread package [40] and a custom GTF file with the coordinates of the overlapping ATAC-seq peak in all the samples used as input for the program. For library normalization and differential accessibility analysis, we used DESeq2. [33]. Differential accessible sites (opening and closing regions) were manually examined in UCSC Genome Browser with the 2019 update (http://genome.ucsc.edu). For enrichment analysis and generating normalized heatmaps and signal intensity plots, we used “deepTools” [41].

ChromHMM analysis

We used ChromHMM algorithm to characterize neuronal chromatin state and the functional chromatin domains at CHD8 targets. We obtained histone mark ChIP-seq data of H9 derived neurons from ENCODE portal [42]. The histone signals binarized across the genome to build a multivariate hidden Markov model and to learn the combinatorial and spatial pattern of histone modification at CHD8 target regions[13].

ChIP quantitative PCR (ChIP-qPCR) experiment

Total 5-10 ng ChIP DNA and the input were used to perform a quantitative PCR experiment and measure the enrichment levels. All primers used are listed in "ChIP-seq-peaks.xlsx" file (attached to GSE141085), along with the relevant information, including the closest gene and the number of the motif on the peak. For each peak site, 3 independent technical replicates (independent IP experiments) were used for qPCR analysis. We normalized the ChIP signal over the input signal, which was less than 0.5% for total IP material. Analysis of qPCR experiment performed on the light Cycler 480II (Roche).

RNA extraction and RT-qPCR experiment for gene expression

For RT-qPCR and RNA-seq experiments, we applied similar RNA isolation methods: neurons that are differentiated on mouse glia cells for ~3 weeks were washed in PBS and then lysed with TRIzol added directly to the plate. RNA was purified with the ZYMO RESEARCH- Direct-zol kit. Human specific primers were used for amplification of desired RNA.

Analysis of dendritic arborizations

Neuronal cultures fixed at approximately 3 weeks after transgene induction with 4% PFA for 15 minutes. The primary and secondary antibodies dilutions are according to our method in

482 “Immunofluorescence experiment”. For morphological analysis and tracing neurites, we used the
483 MetaMorph [43] software and for synaptic puncta analysis and other general image processing, we used
484 java program ImageJand the relevant modules, including CellProfiler 3.0 [44].
485
486 **AAV-mediated gene targeting**
487 For the generation of conditional CHD8 heterozygous knockout cell line we designed a donor vector for
488 homologous recombination that carries two homology arms around the exon 4 of CHD8 gene and
489 included two loxP sequences in the same direction for frameshifting mutation. A positive selection
490 cassette (neomycin expression to confer resistance to Geneticin) included for purifying clones that carry
491 the integrated donor cassette. The selection cassette contained a splice acceptor (SA) and a sequence
492 for internal ribosomal entry site (IRES) attached to Neomycin resistance gene (NEO) and a
493 polyadenylation (PA) signal. The NEO resistant clones were used for screening PCR to verify the
494 correct inserting of the targeting vector in the locus (see Figure S2-2A to 2C). The PCR primers are
495 designed to cover the region from outside the homology arm (primer # 1 and #4) to inside the cassette.
496 The drug resistance cassette was flanked with FRT sequence and later removed by transient
497 expression of FlpE recombinase. For HA-FLAG tagging of CHD8 gene, the tags were inserted into the
498 C-terminus region in the frame before the stop codon of Exon 38, together with the Neomycin
499 resistance gene (see Figure S1-1).
500 After infection of ES cells with recombinant AAV (rAAV-DJ) carrying ITR flanked targeting vectors, we
501 selected the cells with Geneticin antibiotic (Gibco) for ten days or until single colonies were obtained.
502 The resistant colonies expanded, and genomic DNA was extracted for downstream analysis.
503
504 **Electrophysiology**
505 Electrophysiological recordings in cultured iN cells were performed in the whole-cell configuration as
506 described previously [7,45]. Patch pipettes were pulled from borosilicate glass capillary tubes (Warner
507 Instruments) using a PC-10 pipette puller (Narishige). The resistance of pipettes filled with intracellular
508 solution varied between 2-4 MOhm. The standard bath solution contained (in mM): 140 NaCl, 5 KCl, 2

509 $CaCl_2$, 2 $MgCl_2$, 10 HEPES-NaOH pH 7.4, and 10 glucose; 300-305 mosm/l. Excitatory postsynaptic
510 currents (EPSCs) were pharmacologically isolated with picrotoxin (50 μM) and recorded at -70mV
511 holding potential in voltage-clamp mode with a pipette solution containing (in mM): 135 CsCl, 10
512 HEPES-CsOH pH 7.2, 5 EGTA, 4 MgATP, 0.3 Na_4GTP, and 5 QX-314; 295-300 mosm/l. Evoked
513 EPSCs were triggered by 0.5-ms current (100 μA) injection through a local extracellular electrode (FHC
514 concentric bipolar electrode, Catalogue number CBAEC75) placed 100–150μm from the soma of
515 neurons recorded. The frequency, duration, and magnitude of the extracellular stimulus were controlled
516 with a Model 2100 Isolated Pulse Stimulator (A-M Systems, Inc.) synchronized with the Clampex 9 data
517 acquisition software (Molecular Devices). Spontaneous miniature EPSCs (mEPSCs) were monitored in
518 the presence of tetrodotoxin (TTX, 1 μM). mEPSC events were analyzed with Clampfit 9.02 (Molecular
519 Devices) using the template matching search and a minimum threshold of 5pA, and each event was
520 visually inspected for inclusion or rejection. Intrinsic action potential (AP) firing properties of iN cells
521 were recorded in current-clamp mode using a pipette solution that contained (in mM): 123 K-gluconate,
522 10 KCl, 7 NaCl, 1 $MgCl_2$, 10 HEPES-KOH pH 7.2, 1 EGTA, 0.1 $CaCl_2$, 1.5 MgATP, 0.2 Na_4GTP and 4
523 glucose; 295-300 mosm/l. First, minimal currents were introduced to hold membrane potential around
524 −70 mV, next, the increasing amount of currents (from -10 pA to +60 pA, five pA increments) were
525 injected for 1s in a stepwise manner to elicit action potentials. Input resistance (R_{in}) was calculated as
526 the slope of the linear fit of the current-voltage plot generated from a series of small subthreshold
527 current injections. To determine whole-cell membrane capacitance, square wave voltage stimulation
528 was used to produce a pair of decaying exponential current transients that were each analyzed using a
529 least-squares fit technique (Clampfit 9.02). Neuronal excitability recordings were performed using
530 standard bath solution supplemented with 20 μM CNQX, 50 μM AP5, and 50 μM PTX to block all
531 possible glutamatergic (AMPAR- and NMDAR-mediated), as well as GABAergic synaptic transmission.
532 Drugs were applied to the bath solutions prior to all recordings. Data were digitized at 10 kHz with a 2
533 kHz low-pass filter using a Multiclamp 700A amplifier (Molecular Devices). For all electrophysiological
534 experiments, the experimenter was blind to the condition/genotype of the cultures analyzed. All
535 experiments were performed at room temperature.

Quantifications and statistical analysis

All data are shown as means +-SEM and from a minimum of three biological replicates (independent differentiations). GraphPad Prism and R were used for statistical analysis and calculations of significance.

Data and code availability

The raw sequencing files are deposited with the Gene Expression Omnibus (NCBI) (GEO accession number: GSE141085). The list of Encode data used in this study listed in “the ChIP-seq-peaks.xlsx” file (attached to GSE141085).

Competing interest declaration

The authors declare no competing interests.

References

1. Sanders, S.J. *et al.* De novo mutations revealed by whole-exome sequencing are strongly associated with autism. *Nature* **485**, 237-41 (2012).
2. O'Roak, B.J. *et al.* Multiplex targeted sequencing identifies recurrently mutated genes in autism spectrum disorders. *Science* **338**, 1619-22 (2012).
3. O'Roak, B.J. *et al.* Sporadic autism exomes reveal a highly interconnected protein network of de novo mutations. *Nature* **485**, 246-50 (2012).
4. Neale, B.M. *et al.* Patterns and rates of exonic de novo mutations in autism spectrum disorders. *Nature* **485**, 242-5 (2012).
5. Cruzalegui, F.H., Cano, E. & Treisman, R. ERK activation induces phosphorylation of Elk-1 at multiple S/T-P motifs to high stoichiometry. *Oncogene* **18**, 7948-57 (1999).
6. Hawrylycz, M.J. *et al.* An anatomically comprehensive atlas of the adult human brain transcriptome. *Nature* **489**, 391-399 (2012).
7. Zhang, Y. *et al.* Rapid single-step induction of functional neurons from human pluripotent stem cells. *Neuron* **78**, 785-98 (2013).
8. de Dieuleveult, M. *et al.* Genome-wide nucleosome specificity and function of chromatin remodellers in ES cells. *Nature* **530**, 113-6 (2016).
9. Wang, P. *et al.* CRISPR/Cas9-mediated heterozygous knockout of the autism gene CHD8 and characterization of its transcriptional networks in cerebral organoids derived from iPS cells. *Mol Autism* **8**, 11 (2017).
10. Wade, A.A., Lim, K., Catta-Preta, R. & Nord, A.S. Common CHD8 Genomic Targets Contrast With Model-Specific Transcriptional Impacts of CHD8 Haploinsufficiency. *Front Mol Neurosci* **11**, 481 (2018).
11. Abrahams, B.S. *et al.* SFARI Gene 2.0: a community-driven knowledgebase for the autism spectrum disorders (ASDs). *Mol Autism* **4**, 36 (2013).
12. Andersson, R. *et al.* An atlas of active enhancers across human cell types and tissues. *Nature* **507**, 455-461 (2014).
13. Davis, C.A. *et al.* The Encyclopedia of DNA elements (ENCODE): data portal update. *Nucleic Acids Res* **46**, D794-d801 (2018).
14. Jolma, A. *et al.* DNA-binding specificities of human transcription factors. *Cell* **152**, 327-39 (2013).
15. Buenrostro, J.D., Giresi, P.G., Zaba, L.C., Chang, H.Y. & Greenleaf, W.J. Transposition of native chromatin for fast and sensitive epigenomic profiling of open chromatin, DNA-binding proteins and nucleosome position. *Nat Methods* **10**, 1213-8 (2013).
16. Schep, A.N. *et al.* Structured nucleosome fingerprints enable high-resolution mapping of chromatin architecture within regulatory regions. *Genome Res* **25**, 1757-70 (2015).
17. Davies, D.R., Goryshin, I.Y., Reznikoff, W.S. & Rayment, I. Three-dimensional structure of the Tn5 synaptic complex transposition intermediate. *Science* **289**, 77-85 (2000).
18. An integrated encyclopedia of DNA elements in the human genome. *Nature* **489**, 57-74 (2012).
19. Ernst, J. & Kellis, M. Chromatin-state discovery and genome annotation with ChromHMM. *Nat Protoc* **12**, 2478-2492 (2017).
20. Maroulakou, I.G. & Bowe, D.B. Expression and function of Ets transcription factors in mammalian development: a regulatory network. *Oncogene* **19**, 6432-42 (2000).
21. Dolmetsch, R.E., Pajvani, U., Fife, K., Spotts, J.M. & Greenberg, M.E. Signaling to the nucleus by an L-type calcium channel-calmodulin complex through the MAP kinase pathway. *Science* **294**, 333-9 (2001).
22. Thomas, G.M. & Huganir, R.L. MAPK cascade signalling and synaptic plasticity. *Nat Rev Neurosci* **5**, 173-83 (2004).
23. Yu, G., Wang, L.G., Yan, G.R. & He, Q.Y. DOSE: an R/Bioconductor package for disease ontology semantic and enrichment analysis. *Bioinformatics* **31**, 608-9 (2015).
24. Heinz, S. *et al.* Simple combinations of lineage-determining transcription factors prime cis-regulatory elements required for macrophage and B cell identities. *Mol Cell* **38**, 576-89 (2010).

25. Bailey, T.L. *et al.* MEME SUITE: tools for motif discovery and searching. *Nucleic Acids Res* **37**, W202-8 (2009).
26. SPARK: A US Cohort of 50,000 Families to Accelerate Autism Research. *Neuron* **97**, 488-493 (2018).
27. Pang, Z.P. *et al.* Induction of human neuronal cells by defined transcription factors. *Nature* **476**, 220-3 (2011).
28. Lisowski, L. *et al.* Selection and evaluation of clinically relevant AAV variants in a xenograft liver model. *Nature* **506**, 382-6 (2014).
29. Strobel, B. *et al.* Standardized, Scalable, and Timely Flexible Adeno-Associated Virus Vector Production Using Frozen High-Density HEK-293 Cell Stocks and CELLdiscs. *Hum Gene Ther Methods* **30**, 23-33 (2019).
30. Kim, D. *et al.* TopHat2: accurate alignment of transcriptomes in the presence of insertions, deletions and gene fusions. *Genome Biol* **14**, R36 (2013).
31. Li, H. *et al.* The Sequence Alignment/Map format and SAMtools. *Bioinformatics* **25**, 2078-9 (2009).
32. Anders, S., Pyl, P.T. & Huber, W. HTSeq--a Python framework to work with high-throughput sequencing data. *Bioinformatics* **31**, 166-9 (2015).
33. Love, M.I., Huber, W. & Anders, S. Moderated estimation of fold change and dispersion for RNA-seq data with DESeq2. *Genome Biol* **15**, 550 (2014).
34. Rada-Iglesias, A. *et al.* A unique chromatin signature uncovers early developmental enhancers in humans. *Nature* **470**, 279-83 (2011).
35. Chen, X. *et al.* Joint single-cell DNA accessibility and protein epitope profiling reveals environmental regulation of epigenomic heterogeneity. *Nat Commun* **9**, 4590 (2018).
36. Buenrostro, J.D., Wu, B., Chang, H.Y. & Greenleaf, W.J. ATAC-seq: A Method for Assaying Chromatin Accessibility Genome-Wide. *Curr Protoc Mol Biol* **109**, 21.29.1-9 (2015).
37. de Hoon, M.J., Imoto, S., Nolan, J. & Miyano, S. Open source clustering software. *Bioinformatics* **20**, 1453-4 (2004).
38. Saldanha, A.J. Java Treeview--extensible visualization of microarray data. *Bioinformatics* **20**, 3246-8 (2004).
39. Huang da, W., Sherman, B.T. & Lempicki, R.A. Systematic and integrative analysis of large gene lists using DAVID bioinformatics resources. *Nat Protoc* **4**, 44-57 (2009).
40. Liao, Y., Smyth, G.K. & Shi, W. featureCounts: an efficient general purpose program for assigning sequence reads to genomic features. *Bioinformatics* **30**, 923-30 (2014).
41. Ramirez, F. *et al.* deepTools2: a next generation web server for deep-sequencing data analysis. *Nucleic Acids Res* **44**, W160-5 (2016).
42. Ernst, J. & Kellis, M. ChromHMM: automating chromatin-state discovery and characterization. *Nat Methods* **9**, 215-6 (2012).
43. Wallace, W. & Bear, M.F. A morphological correlate of synaptic scaling in visual cortex. *J Neurosci* **24**, 6928-38 (2004).
44. McQuin, C. *et al.* CellProfiler 3.0: Next-generation image processing for biology. *PLoS Biol* **16**, e2005970 (2018).
45. Maximov, A. & Sudhof, T.C. Autonomous function of synaptotagmin 1 in triggering synchronous release independent of asynchronous release. *Neuron* **48**, 547-54 (2005).

Main Figures

Fig. 1

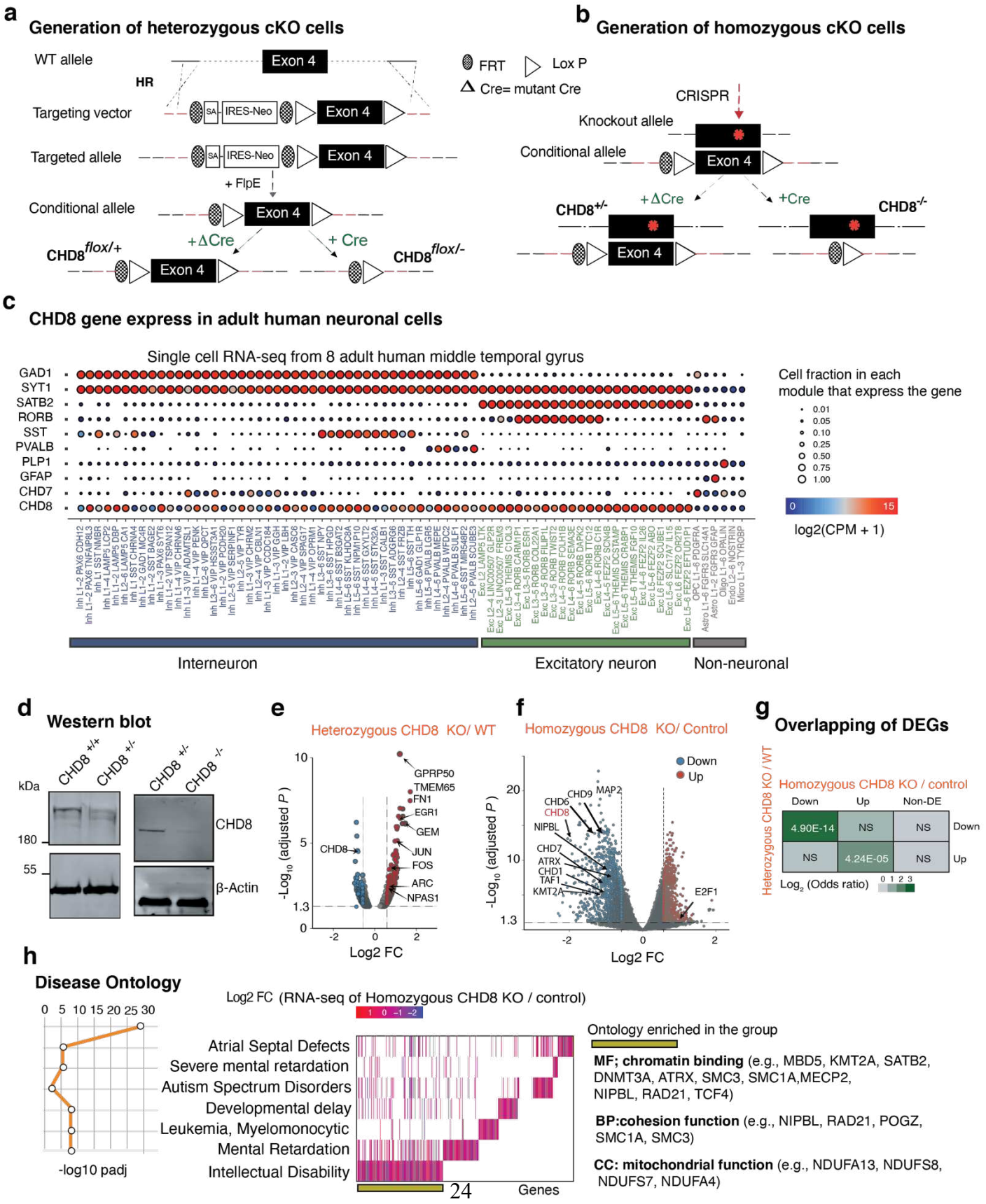

Fig. 2

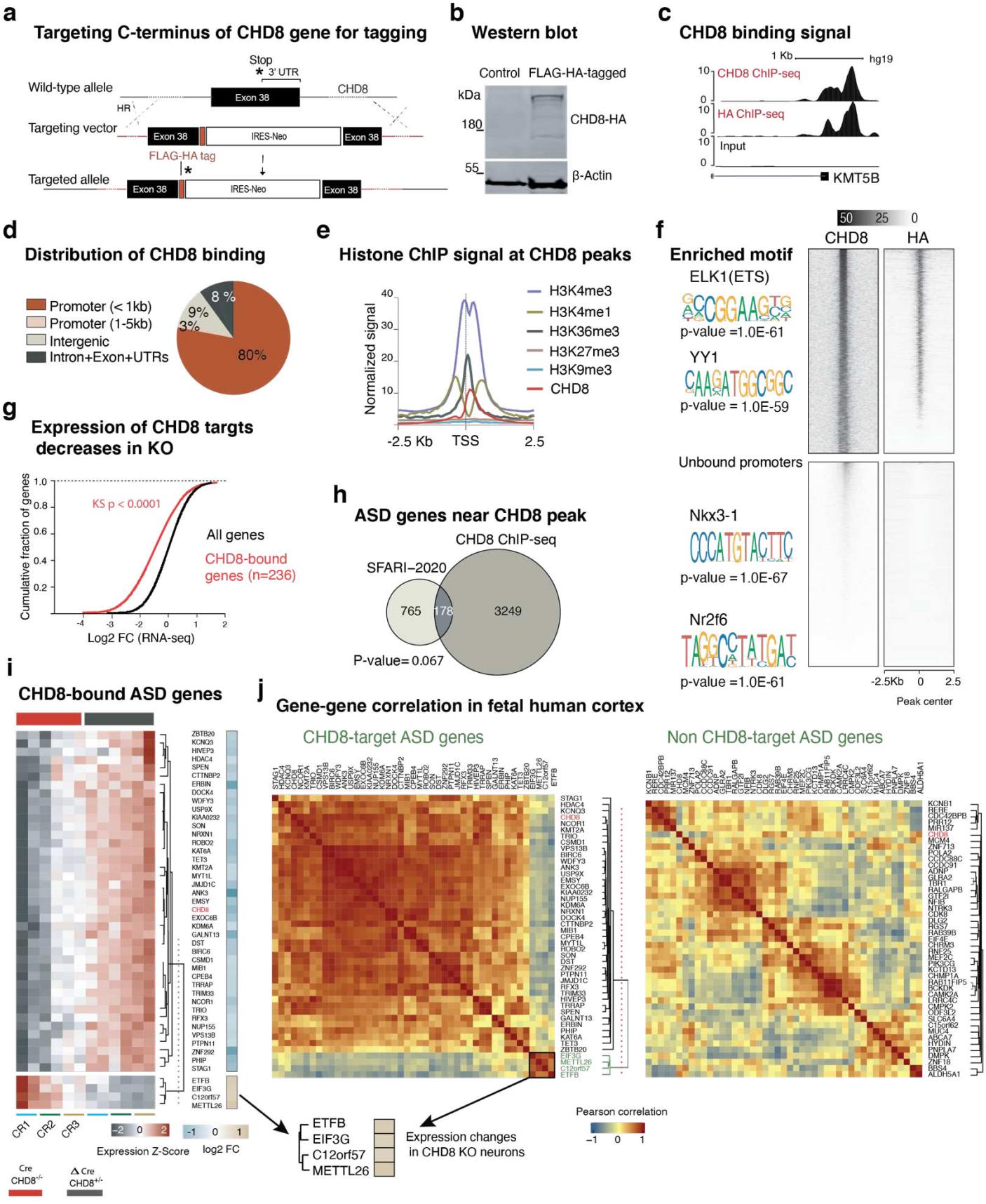
a
Targeting C-terminus of CHD8 gene for tagging
Stop
3' UTR
Wild-type allele
Exon 38
CHD8
HR
Targeting vector
Exon 38
IRES-Neo
Exon 38
FLAG-HA tag
Targeted allele
Exon 38
IRES-Neo
Exon 38
b
Western blot
Control
FLAG-HA-tagged
kDa
180
CHD8-HA
55
β-Actin
c
CHD8 binding signal
1 Kb
hg19
CHD8 ChIP-seq
HA ChIP-seq
Input
KMT5B
d
Distribution of CHD8 binding
Promoter (< 1kb)
Promoter (1-5kb)
Intergenic
Intron+Exon+UTRs
8 %
9%
3%
80%
e
Histone ChIP signal at CHD8 peaks
Normalized signal
H3K4me3
H3K4me1
H3K36me3
H3K27me3
H3K9me3
CHD8
-2.5 Kb
TSS
2.5
f
Enriched motif
50
25
0
CHD8
HA
ELK1(ETS)
p-value =1.0E-61
YY1
p-value = 1.0E-59
Unbound promoters
Nkx3-1
p-value =1.0E-67
Nr2f6
p-value =1.0E-61
-2.5Kb
0
2.5
Peak center
g
Expression of CHD8 targts decreases in KO
Cumulative fraction of genes
KS p < 0.0001
All genes
CHD8-bound genes (n=236)
Log2 FC (RNA-seq)
h
ASD genes near CHD8 peak
CHD8 ChIP-seq
SFARI-2020
765
178
3249
P-value= 0.067
i
CHD8-bound ASD genes
CR1
CR2
CR3
Expression Z-Score
log2 FC
Cre
CHD8-/-
Δ Cre
CHD8+/-
ETFB
EIF3G
C12orf57
METTL26
Expression changes in CHD8 KO neurons
j
Gene-gene correlation in fetal human cortex
CHD8-target ASD genes
Non CHD8-target ASD genes
Pearson correlation

663 **Fig. 3**

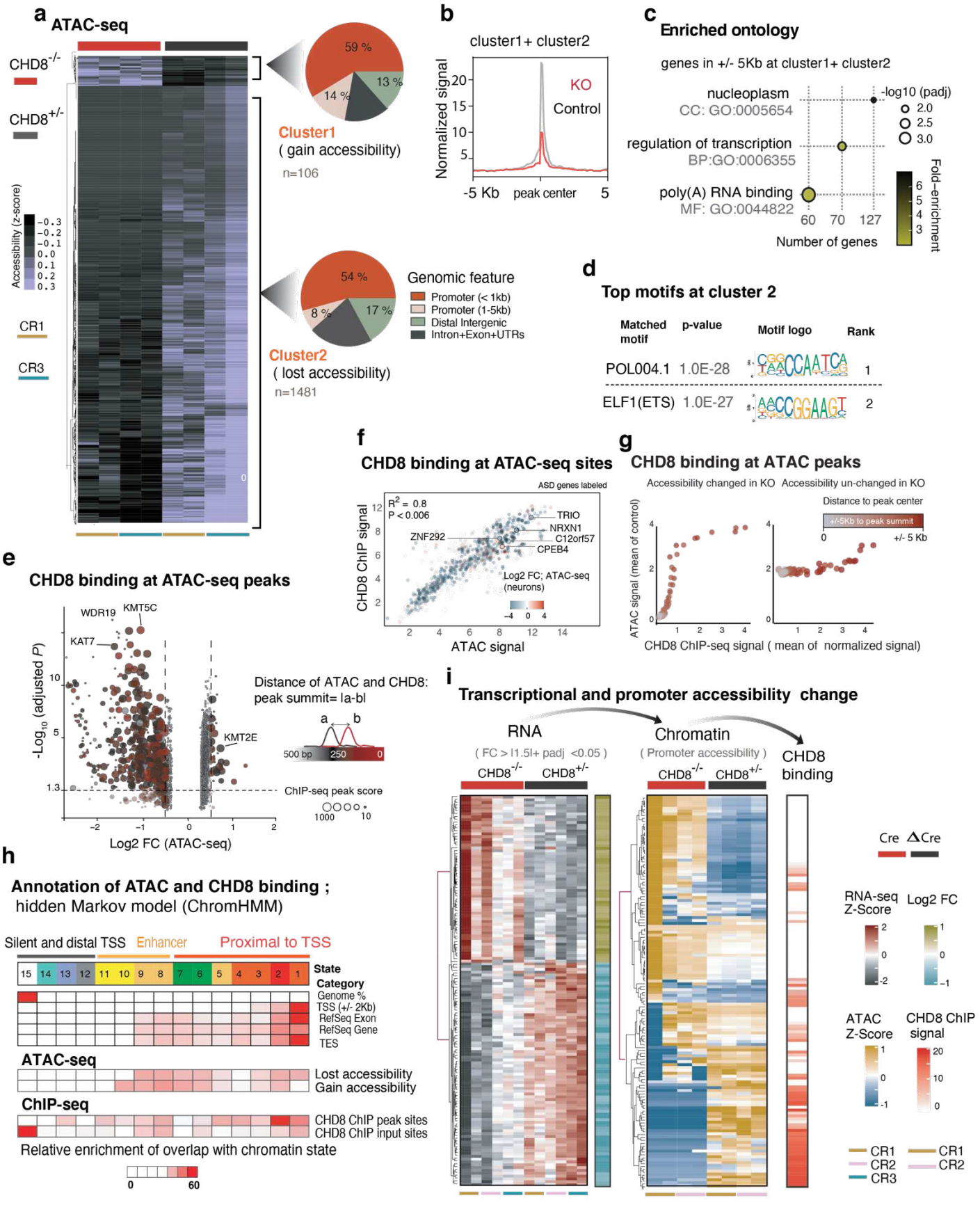
a
ATAC-seq
CHD8-/-
CHD8+/-
Accessibility (z-score)
CR1
CR3
59 %
13 %
14 %
Cluster1
(gain accessibility)
n=106
54 %
8 %
17 %
Cluster2
(lost accessibility)
n=1481
Genomic feature
Promoter (< 1kb)
Promoter (1-5kb)
Distal Intergenic
Intron+Exon+UTRs
b
cluster1+ cluster2
Normalized signal
KO
Control
-5 Kb
peak center
5
c
Enriched ontology
genes in +/- 5Kb at cluster1+ cluster2
nucleoplasm
CC: GO:0005654
regulation of transcription
BP:GO:0006355
poly(A) RNA binding
MF: GO:0044822
-log10 (padj)
Fold-enrichment
Number of genes
d
Top motifs at cluster 2
Matched motif
p-value
Motif logo
Rank
POL004.1 1.0E-28
1
ELF1(ETS) 1.0E-27
2
e
CHD8 binding at ATAC-seq peaks
WDR19
KMT5C
KAT7
KMT2E
-Log10 (adjusted P)
Log2 FC (ATAC-seq)
Distance of ATAC and CHD8:
peak summit= Ia-bI
500 bp
ChIP-seq peak score
f
CHD8 binding at ATAC-seq sites
ASD genes labeled
R2 = 0.8
P < 0.006
ZNF292
TRIO
NRXN1
C12orf57
CPEB4
Log2 FC; ATAC-seq (neurons)
CHD8 ChIP signal
ATAC signal
g
CHD8 binding at ATAC peaks
Accessibility changed in KO
Accessibility un-changed in KO
Distance to peak center
+/-5Kb to peak summit
+/- 5 Kb
ATAC signal (mean of control)
CHD8 ChIP-seq signal (mean of normalized signal)
h
Annotation of ATAC and CHD8 binding ;
hidden Markov model (ChromHMM)
Silent and distal TSS
Enhancer
Proximal to TSS
State
Category
Genome %
TSS (+/- 2Kb)
RefSeq Exon
RefSeq Gene
TES
ATAC-seq
Lost accessibility
Gain accessibility
ChIP-seq
CHD8 ChIP peak sites
CHD8 ChIP input sites
Relative enrichment of overlap with chromatin state
i
Transcriptional and promoter accessibility change
RNA
(FC > I1.5I+ padj <0.05)
Chromatin
(Promoter accessibility)
CHD8 binding
CHD8-/-
CHD8+/-
Cre
ΔCre
RNA-seq Z-Score
Log2 FC
ATAC Z-Score
CHD8 ChIP signal
CR1
CR2
CR3

Fig. 4

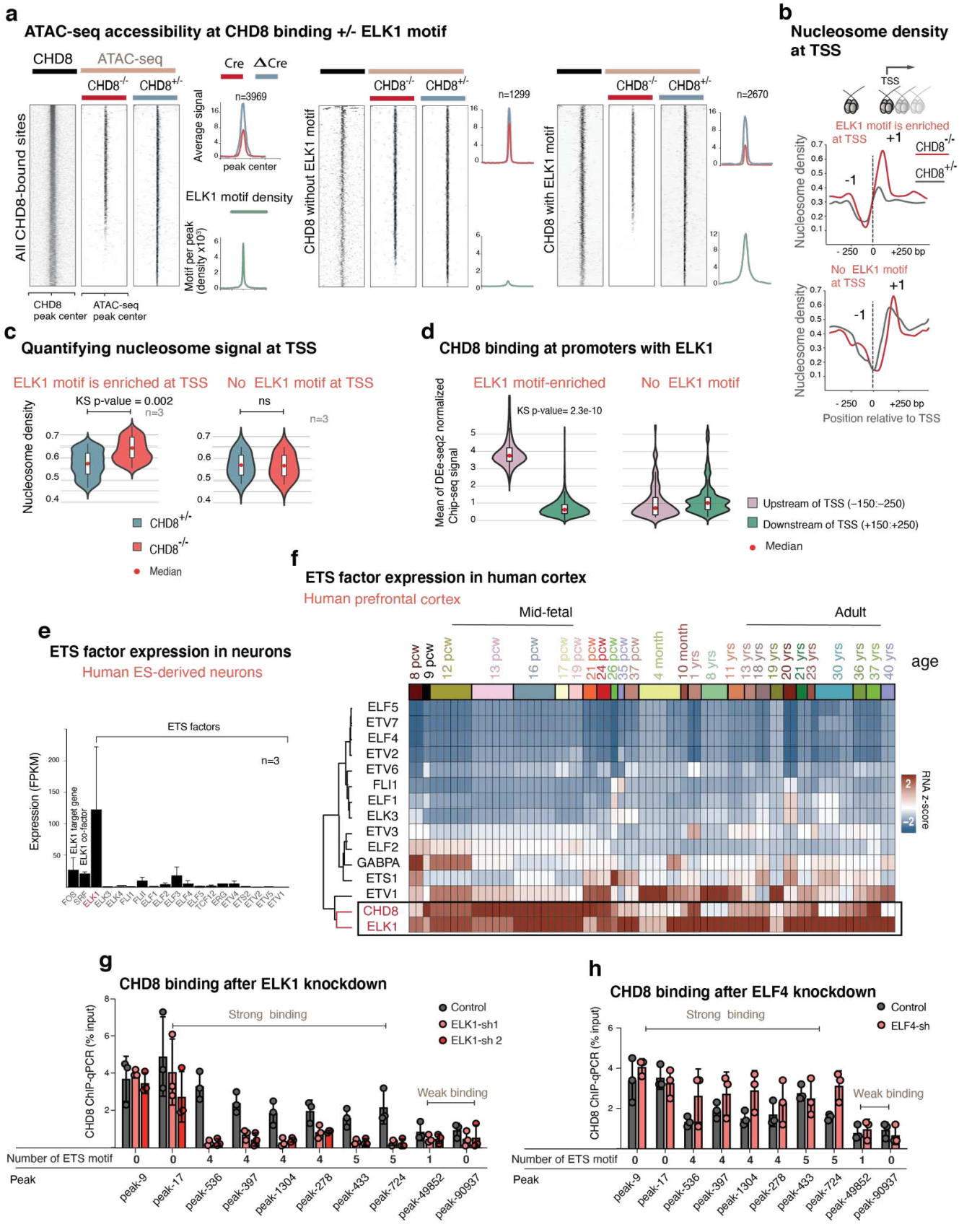
a
ATAC-seq accessibility at CHD8 binding +/- ELK1 motif
CHD8
ATAC-seq
CHD8-/-
CHD8+/-
Cre
ΔCre
All CHD8-bound sites
Average signal
n=3969
peak center
ELK1 motif density
Motif per peak (density x10³)
CHD8 peak center
ATAC-seq peak center
CHD8 without ELK1 motif
n=1299
CHD8 with ELK1 motif
n=2670
b
Nucleosome density at TSS
TSS
ELK1 motif is enriched at TSS
+1
-1
Nucleosome density
- 250
0
+250 bp
No ELK1 motif at TSS
Position relative to TSS
c
Quantifying nucleosome signal at TSS
ELK1 motif is enriched at TSS
No ELK1 motif at TSS
KS p-value = 0.002
n=3
ns
Nucleosome density
CHD8+/-
CHD8-/-
Median
d
CHD8 binding at promoters with ELK1
ELK1 motif-enriched
No ELK1 motif
KS p-value= 2.3e-10
Mean of DEe-seq2 normalized Chip-seq signal
Upstream of TSS (−150:−250)
Downstream of TSS (+150:+250)
Median
e
ETS factor expression in neurons
Human ES-derived neurons
ETS factors
n=3
Expression (FPKM)
ELK1 target gene
ELK1 co-factor
FOS SRF ELK1 ELK3 ELK4 FLI1 ELF1 ELF2 ELF3 ELF4 ELF5 TCF12 ERG ETV4 ETS2 ETV2 ETV5 ETV1
f
ETS factor expression in human cortex
Human prefrontal cortex
Mid-fetal
Adult
age
8 pcw
9 pcw
12 pcw
13 pcw
16 pcw
17 pcw
19 pcw
21 pcw
24 pcw
26 pcw
35 pcw
37 pcw
4 month
10 month
1 yrs
8 yrs
11 yrs
13 yrs
18 yrs
19 yrs
20 yrs
21 yrs
23 yrs
30 yrs
36 yrs
37 yrs
40 yrs
ELF5
ETV7
ELF4
ETV2
ETV6
FLI1
ELF1
ELK3
ETV3
ELF2
GABPA
ETS1
ETV1
CHD8
ELK1
RNA z-score
g
CHD8 binding after ELK1 knockdown
CHD8 ChIP-qPCR (% input)
Strong binding
Weak binding
Control
ELK1-sh1
ELK1-sh 2
Number of ETS motif
Peak
peak-9
peak-17
peak-536
peak-397
peak-1304
peak-278
peak-433
peak-724
peak-49852
peak-90937
h
CHD8 binding after ELF4 knockdown
CHD8 ChIP-qPCR (% input)
Strong binding
Weak binding
Control
ELF4-sh
Number of ETS motif
Peak

Supplementary Files

This is a list of supplementary files associated with this preprint. Click to download.

- SupplementaryExtendedDataFiguresandLegends.pdf